THE STUDY OF THE ANISOTROPY OF POLYCRYSTALLINE FERROMAGNETIC MATERIALS BY MEANS OF THE MICROWAVE RESONANCE METHOD

Thesis for the Degree of M. S.

MICHIGAN STATE COLLEGE

William Franklin Heckert

1950

This is to certify that the

thesis entitled

The Study of the Anisotropy of Poly-crystalline Ferromagentic Materials by Means of the Micro-wave Resonance Method

presented by

William F. Heckert

has been accepted towards fulfillment
of the requirements for

M.S. degree in Physics

Robert D Spence
Major professor

Date 23 May 1950

O-169

THE STUDY OF THE ANISOTROPY OF POLYCRYSTALLINE FERROMAGNETIC MATERIALS BY MEANS OF THE MICROWAVE RESONANCE METHOD

by

William Franklin Heckert

A THESIS

Submitted to the School of Graduate Studies of Michigan State College of Agriculture and Applied Science in partial fulfillment of the requirements for the degree of MASTER OF SCIENCE

Department of Physics

1950

ACKNOWLEDGMENT

I wish to thank Dr. Robert D. Spence, under whose direction this work was done, for his many helpful suggestions and patient guidance throughout the course of the problem. I would also like to thank Mr. Charles Kingston for his work on the construction of apparatus.

William F. Heckert

TABLE OF CONTENTS

I. Introduction

Ferromagnetic Resonance Absorption was originally observed by J. H. E. Griffiths[1] in 1946 and since then considerable work has been reported by other investigators. Among these are Yager and Bozorth[2], Kip and Arnold[3], and Kittel[4].

A ferromagnetic sample is used as one wall of a rectangular resonant cavity which terminates a waveguide section. The other end of the waveguide is connected to a microwave oscillator which delivers microwave power to the resonant cavity. The ferromagnetic material is so placed in the cavity that the magnetic vector of the microwave field is constant in direction in the sample. An electromagnet is used to furnish a static magnetic field which is applied in the plane of the sample of the resonant cavity and at 90° to the r.f. magnetic field. Directional couplers inserted between the cavity and oscillator provide means of coupling reflected power to suitable detection apparatus.

When the strength of the magnetic field is increased, one observes that the r.f. energy loss in the cavity goes through a maximum. When the power loss is plotted as a function of magnetic field strength a resonance curve is obtained

---

1. J.H.E.Griffiths, Nature 158, 670 (1946)
2. W.A.Yager and R.M.Bozorth, Phys. Rev. 72, 80 (1947)
3. A.F.Kip and R.D.Arnold, Phys. Rev. 75, 1556 (1949)
4. C.Kittel, Phys. Rev., 73, 155 (1948)

whose general appearance is shown in Figure 1.

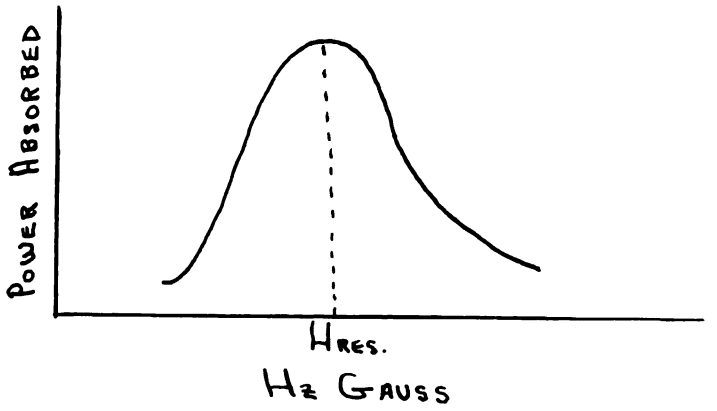

Figure 1

The field at which maximum power loss is observed is called the resonance field. In Figure 1, this value is designated by H_{res}.

Ferromagnetic materials are anisotropic and, therefore, different magnetizing forces are required to magnetize them to saturation in different directions with respect to the crystal axes. Kip and Arnold have found that the resonance fields are dependent on the orientation of the crystal axes with respect to the magnetic field. Their experiments were conducted with a single crystal of iron.

It is the purpose of this experiment to study the anisotropy of polycrystalline ferromagnetic materials by the resonance absorption method. We shall investigate the resonance fields for different orientations of the 100 direction in Silectron with respect to the static magnetic field.

II. Theory

We shall first consider resonance absorption from a simple spectroscopic point of view.

Ferromagnetic materials have been found to have essentially zero electronic orbital angular momentum and the only angular momentum of significance is that due to electron spin. According to Weiss, an unmagnetized ferromagnetic material is divided into small domains which are magnetized to saturation. The sum of the individual spins is equal to the total domain angular momentum as given by this relation

$$(1)\quad \vec{M} = \hbar \sum_i \vec{s}_i$$

where $\vec{M}$ = domain angular momentum and $\vec{s}_i$ = electron spin.

If a magnetic field H of sufficient strength is applied, the domain spins will all line up in the field direction and the specimen will be magnetized as a single domain. We also note that the large angular momentum due to spin is quantized with respect to an axis parallel to the static magnetic field.

An occasional spin will be oriented anti-parallel to the field and will decrease the angular momentum vector $\vec{M}$. Figure 2 shows the quantization of $\vec{M}$ with H.

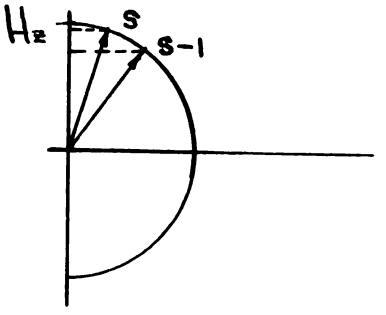

Figure 2

While this lone spin is so oriented we will have two energy levels looking something like this:

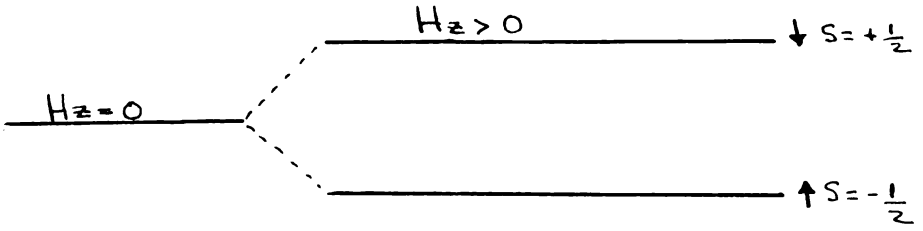

Figure 3

The difference in energy which gives the two energy levels follows from a simple classical argument: When a spin is oriented as shown in Figure 4

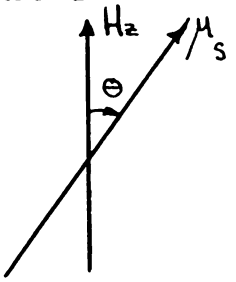

Figure 4

with a magnetic moment $\vec{\mu}_s$, its energy is given by the relation

$$(2)\quad E = -\vec{\mu}_s \cdot \vec{H} = -\mu_s H \cos\theta$$

If $\vec{\mu}_s$ is oriented parallel to the field direction, we have the most stable energy state and therefore a lower energy than if $\vec{\mu}_s$ were oriented anti-parallel to H in which case we would have a higher and, consequently, less stable energy state.

The resonance condition occurs when we have a transition from an energy level having a lower energy to one having higher energy; in this case when the spin vector parallel to the field is "flipped" over to position where the vector is anti-parallel to the field.

The reversal of the spin is accomplished by the microwave magnetic field and the energy required to "flip" these vectors accounts for the energy loss in the resonant cavity as the static magnetic field is varied. The relaxation time is very short so the relaxation mechanism establishes a surplus in the lower state and absorption occurs rather than emission.

The energy which the radio frequency field must supply to reverse the spin is given by the equation

$$(3)\quad \Delta E = h\nu_{r.f.}$$

This energy is constant in value and transitions between energy levels occur when the difference in energy of the two levels is equal to $h\nu_{r.f.}$

The expression for energy difference between the two levels represented by oppositely oriented spins is equal to

$$(4)\quad g\mu_B H_z = h\nu_{r.f.}$$

and is represented diagrammatically by Figure 5.

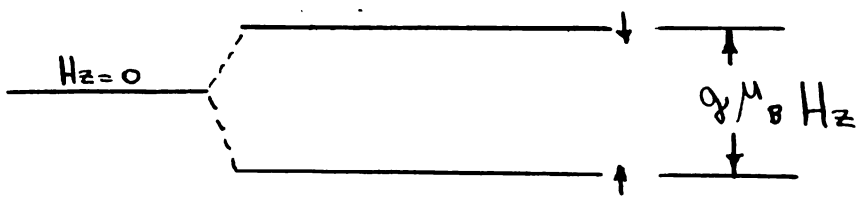

Figure 5

If our line widths were of infinitely narrow width in Figure 5, the transitions, theoretically, would occur for only one value of Hz and the absorption curve would be infinitely sharp. However, the lines are of finite widths and consequently

transitions can occur for more than one value of Hz. Thus we get a resonance curve similar to the one shown on page 2. That is, we get transitions other than at the point given by equation (4).

The finite line width can be explained in the following way: The field in the interior of the specimen is not quite what one would expect from classical predictions, obtained by taking the shape of the specimen into account. This happens because the local fields in the neighborhood of individual spins vary as the spins are "flipped" from one position to another. Thus, at one instant of time, the actual field near a particular spin may be slightly greater than the internal field and a neighboring spin may have an actual field of slightly lower value than the internal field predicted in the previously-mentioned manner. It is now obvious that in a given specimen we will have spins of varying energy i.e. many of the higher-energy spins will vary a little above and a little below the average energy for that level. The same will hold for the lower energy levels and it will be possible for a variety of transitions to occur instead of a single type from one energy level to another. However, most of the transitions will occur at the predicted field values. Thus we see that the resonance curve will be of a finite width rather than a single vertical line.

Returning to equation (4) which is

$$(4)\quad h\nu_{r.f.} = g\mu_B H_z$$

one can easily see that

$$(5)\quad \omega_{n.f.} = g\frac{e}{2mc} H_z$$

where g is the Lande' g factor and is equal to 2 for a free spin. Setting g = 2, we obtain

$$(6)\quad \omega_{n.f.} = \frac{e}{mc} H_z$$

This equation is just equal to the Larmor frequency condition

$$(7)\quad \omega = \gamma H_z$$

where γ = e/mc and is commonly called the magneto-mechanical ratio.

The Larmor precession may be also used to interpret the resonance phenomenon. By Larmor precession we mean the precession of the electron spin vector about the applied static field direction. The resonance phenomenon can be thought of as occurring when the frequency of the microwave field is equal to the Larmor frequency. While this method of deriving the angular frequency relation is not the one we have used, the method gives identical results. Therefore, when thinking of ferromagnetic resonance absorption, one can think of the method we have outlined or the Larmor precession about the field direction.

We shall now consider the effect of the shape of the specimen on the resonance condition. The field inside the specimen is modified by a demagnetization field which materially alters the field present in the interior. Thus the

internal field will not be $\vec{H}_z$ but $\vec{H}_i$. The two are related by

$$(8)\quad \vec{H}_i = \vec{H}_z - \vec{N}\cdot\vec{M}$$

where $\vec{N}$ is a demagnetization dyadic and $\vec{M}$ is a magnetization vector.

We shall now calculate the resonant frequency for the field given by equation (8). Since the angular momentum of the entire sample is large, we may use the correspondence principle to reduce the problem to a classical one: $\vec{J}$ will be designated as angular momentum density / unit volume. The magnetization $\vec{M}$ and angular momentum density $\vec{J}$ are related by the equation

$$(9)\quad \vec{M} = \gamma \vec{J}$$

The equation of motion / unit volume of material is given by

$$(10)\quad \frac{d\vec{J}}{dt} = \vec{T}$$

where

$$(11)\quad \vec{T} = \vec{M}\times\vec{H}_i + \vec{T}_a$$

and $\vec{T}$ is the torque acting on a unit volume. $\vec{T}_a$ is the anisotropy torque.

Equation (11) becomes

$$(12)\quad \frac{d\vec{M}}{dt} = \gamma\left(\vec{M}\times\vec{H}_i + \vec{T}_a\right)$$

From this relation we can calculate the susceptibility of the radio frequency field.

Let us consider the resonance condition for a general ellipsoid having principal axes parallel to the x, y, and z axes of the Cartesian coordinate system. The demagnetizing factors along these three directions are N_x, N_y, and N_z. The static applied magnetic field is H_z and the microwave field is H_x. The values of $\vec{H}_i$ in these three directions are

$$(13)\quad H_x^i = H_x - N_x M_x$$

$$(14)\quad H_y^i = -N_y M_y$$

$$(15)\quad H_z^i = H_z - N_z M_z$$

and the equation for $\vec{H}_i$ is

$$(16)\quad \vec{H}_i = \vec{i}\,(H_x - N_x M_x) + \vec{j}\,(-N_y M_y) + \vec{k}\,(H_z - N_z M_z)$$

If we substitute these values in the equation of motion we get the three component equations

$$(17)\quad \dot{M}_x = \gamma\left[M_y(H_z - N_z M_z) - M_z(-N_y M_y) + T_{ax}\right]$$

$$(18)\quad \dot{M}_y = \gamma\left[M_z(H_x - N_x M_x) - M_x(H_z - N_z M_z) + T_{ay}\right]$$

$$(19)\quad \dot{M}_z = \gamma\left[M_x(-N_y M_y) - M_y(H_x - N_x M_x) + T_{az}\right]$$

By factoring, we see that

$$(20)\quad \dot{M}_x = \gamma\left[(H_z - N_z M_z + N_y M_z)M_y + T_{ax}\right]$$

$$(21)\quad \dot{M}_y = -\gamma\left(N_x M_z + (H_z - N_z M_z)M_x\right) + \gamma M_z H_x + \gamma T_{ay}$$

$$(22)\quad \dot{M}_z \cong 0$$

We shall call $\dot{M}_z$ equal to zero since no Mz terms appear here and the quantity is therefore very small. (M_x and M_y are small while M_z is large)

Now, we shall assume a time dependence $e^{i\omega t}$

$$(23)\quad M_x(t) = M_x e^{i\omega t}$$

We may call (20) equal to

$$(24)\quad i\omega M_x = \left[\gamma\left(H_z + (N_y - N_z)M_z\right]\right] M_y$$

and (21) equal to

$$(25)\quad i\omega M_y = \left[-\gamma\left(H_z + (N_x - N_z)M_z\right]\right] M_x + \gamma M_z H_x$$

Solving (24) for My gives

$$(26)\quad M_y = \frac{i\omega M_x}{\gamma\left[H_z + (N_y - N_z)M_z\right]}$$

Substituting this My value into (25) we obtain

$$(27)\quad \frac{-\omega^2 M_x}{\gamma\left[H_z + (N_y - N_z)M_z\right]} = -\gamma\left[H_z + (N_x - N_z)M_z\right] M_x + \gamma M_z H_x$$

From (27) manipulation gives

$$(28)\quad \left(\frac{-\omega^2}{\gamma^2\left[(H_z + (N_y - N_z)M_z)(H_z + (N_x - N_z)M_z)\right]} + 1\right) M_x = \frac{\gamma M_z H_x}{\gamma\left[H_z + (N_x - N_z)M_z\right]}$$

Before continuing, we must point out that the components T_{ax} and T_{ay} of the anisotropy torque have been temporarily discarded for convenience of manipulation. Later in this discussion they will be calculated and added to the H_z expressions.

The susceptibility of the r.f. field is given by

$$(29)\quad \chi = \frac{M_x}{H_{r.f.}} = \frac{M_x}{H_x}$$

and

$$(30)\quad \chi = \frac{\dfrac{M_z}{\left[H_z + (N_x - N_z)M_z\right]}}{\left(1 - \dfrac{\omega^2}{\gamma^2\left[(H_z + (N_y - N_z)M_z)(H_z + (N_x - N_z)M_z)\right]}\right)}$$

At resonance $\chi \longrightarrow \infty$

and therefore,

$$(31)\quad \omega^2 = \gamma^2\left[(H_z + (N_y - N_z)M_z)(H_z + (N_x - N_z)M_z)\right]$$

where ω is the resonance frequency i.e. the frequency of the r.f. field.

We now consider special cases of equation (31), showing how (31) varies depending on the shape of the ferromagnetic specimen.

For a plane, which is the type of sample we have used here, the demagnetizing factors are $N_x = N_z = 0$; $N_y = 4\pi$. Then

$$(32)\quad \omega^2 = \gamma^2\left[(H_z + 4\pi M_z)(H_z)\right]$$

For a sphere, $N_x = N_y = N_z = 4\pi/3$ and the resonance equation reduces to

$$(33)\quad \omega^2 = \gamma^2 H_z^2 \quad \text{or} \quad \omega = \gamma H_z$$

which is the simple Larmor expression.

It is of interest to note also that the magnetization vector $M_z = 1700$ gauss for iron.

Having shown that the resonance condition changes with the shape of the specimen, we may now consider the effect of

crystalline anisotropy on the resonance condition. We may start this by discussing crystalline anisotropy briefly.

In a ferromagnetic crystal there is a variation of magnetic properties with direction. If we consider iron, we see that iron crystals are of a body-centered cubic structure

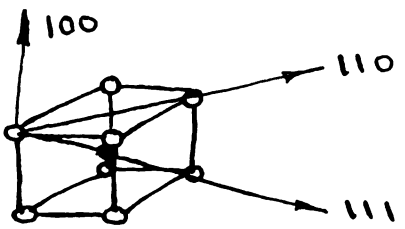

Figure 6

in which 100, 110, and 111 are directions with respect to the crystal axes. The 100 direction is known as the direction of easy magnetization, and the 110 as the direction of medium magnetization and the 111 the direction of hard magnetization. In a face-centered cubic crystal such as nickel, the roles of the 100 and 111 directions are reversed from their properties in iron.

These variations in magnetization with direction can be shown in a series of magnetization curves drawn for these three directions

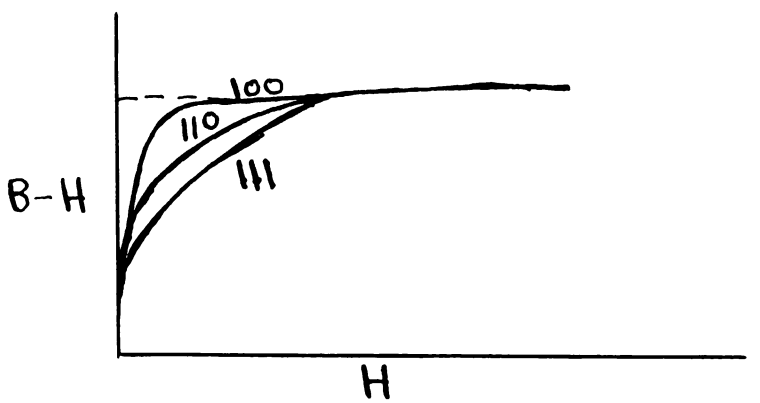

Figure 7

The internal energy density of ferromagnetic crystals depends on the direction of magnetization relative to the crystal axes and is called the anisotropy energy.

The direction of magnetization is defined by the direction cosines S_1, S_2 and S_3 referred to the cubic axes of the crystal. We can expand the energy in a power series of direction cosines and get

$$(34)\quad E = K_0 + K_1\left(S_1^2S_2^2 + S_2^2S_3^2 + S_3^2S_1^2\right) + K_2\left(S_1^2S_2^2S_3^2\right)$$

The major term in the anisotropy energy is the portion

$$(35)\quad E_m = K_1\left(S_1^2S_2^2 + S_2^2S_3^2 + S_3^2S_1^2\right)$$

The anisotropy energy will cause a change in the resonance condition. In a single ferromagnetic crystal the magnetic field required to produce resonance will vary, depending on the direction of the crystal axes with respect to the magnetization of the sample. In a polycrystalline specimen, such as the Silectron used in this experiment, one would expect a resonance condition which is much broader than that of the single crystal. This broadness is introduced by the distribution in direction of the crystal axes which in turn introduces a distribution in field strengths required for the resonance absorption.

On page 10 we temporarily abandoned the torques T_{ax} and T_{ay}. We shall now calculate T_{ax} and T_{ay} from mechanics by using the relations

$$(36)\quad \vec{T} = \vec{\mathcal{M}} \times \vec{F} = -\vec{\mathcal{M}} \times \vec{\nabla} E = \vec{\nabla} \times (\vec{\mathcal{M}} E)$$

and

$$(37)\quad E = K_1 \left(S_1^2 S_2^2 + S_2^2 S_3^2 + S_1^2 S_3^2 \right)$$

where $\vec{T}$ is the torque due to anisotropy and E is the major part of the anisotropy energy. Equation (37) is identical with equation (35).

The metal used in this experiment was a highly anisotropic metal known as Silectron which has its rolling direction along the 110 direction and we shall use this fact to derive the anisotropy torques in the x and y directions.

Figure 8 shows the coordinate system used to describe the Silectron and its position, in our experimental arrangement, with respect to H_Z and H_X.

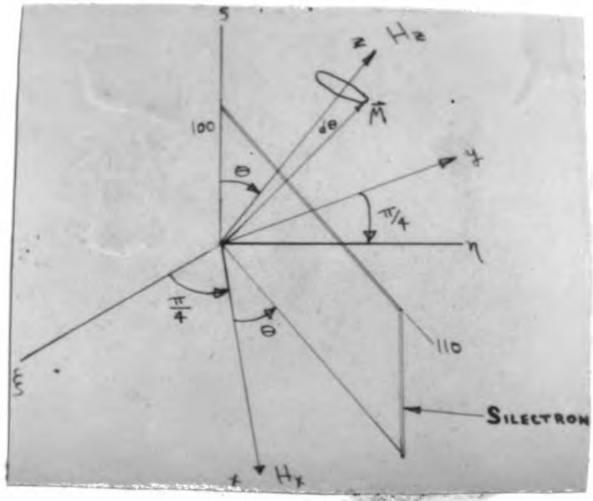

Figure 8

This drawing represents two Cartesian coordinate systems in ξ, η, S and x, y, and z.

The direction cosines of the energy given in equation

(37) are

$$(38)\quad S_1 = \frac{M_\xi}{M} \quad , \quad S_2 = \frac{M_\eta}{M} \quad , \quad S_3 = \frac{M_\zeta}{M}$$

So (37) now becomes

$$(39)\quad E = \frac{K_1}{M^4}\left(M_\xi^2 M_\eta^2 + M_\xi^2 M_\zeta^2 + M_\eta^2 M_\zeta^2\right)$$

From Figure 8, we can find the values of M_ξ, M_η, and M_ζ components.

$$(40)\quad M_\xi = \frac{\cos\theta}{\sqrt{2}} M_x - \frac{1}{\sqrt{2}} M_y + \frac{\sin\theta}{\sqrt{2}} M_z$$

$$(41)\quad M_\eta = \frac{\cos\theta}{\sqrt{2}} M_x + \frac{1}{\sqrt{2}} M_y + \frac{\sin\theta}{\sqrt{2}} M_z$$

$$(42)\quad M_\zeta = -\sin\theta M_x + \cos\theta M_z$$

Now, we must square these three values and place the results in equation (39). We may simplify the energy expression somewhat by discarding all terms not containing M_z i.e. all terms in M_x and M_y alone.

The energy is given by

$$(43)\quad E = K_1\left[\left(-3\sin^2\theta\cos^2\theta\right)\frac{M_x^2 M_z^2}{M^4} + \left(2\sin\theta\cos^3\theta - \sin^3\theta\cos\theta\right)\frac{M_x M_z^3}{M^4} - \sin^2\theta\frac{M_y^2 M_z^2}{M^4} + \left(\frac{\sin^4\theta}{4} + \sin^2\theta\cos^2\theta\right)\frac{M_z^4}{M^4}\right]$$

Setting Mz = M, (43) becomes

$$(44)\quad E = K_1\left[\left(-3\sin^2\theta\cos^2\theta\right)\frac{M_x^2}{M^2} + \left(2\sin\theta\cos^3\theta - \sin^3\theta\cos\theta\right)\frac{M_x}{M} - \sin^2\theta\frac{M_y^2}{M^2} + \left(\frac{\sin^4\theta}{4} + \sin^2\theta\cos^2\theta\right)\right]$$

To conserve space, we shall indicate what the next few steps

are:

1) The gradient of E is computed

2) $\vec{r}$ is crossed into $\vec{\nabla} E$ giving us an equation for torque. This torque equation will be in the f orm

$$(45) \quad \vec{T}a = \vec{i}\, T_{ax} + \vec{j}\, T_{ay} + \vec{k}\, T_{az}$$

Since we are interested in only T_{ax} and T_{ay}, we see that these components are equal to

$$(46) \quad T_{ax} = 2K_1 \sin^2\theta \frac{M_y}{M}$$

$$(47) \quad T_{ay} = -6K_1 \sin^2\theta \cos^2\theta \frac{M_x}{M} + 2K_1 \sin\theta \cos^3\theta - K_1 \sin^3\theta \cos\theta$$

We now return to where we dropped the T_{ax} and T_{ay} components of the equation of motion. Equations (46) and (47) are placed in equations (20) and (21). The solution of the resonance formula, equation (31), will then equal

$$(48) \quad \omega^2 = \gamma^2 \left[\left(H_z + (N_y - N_z) M_z + \frac{2K_1 \sin^2\theta}{M_z} \right) \left(H_z + (N_x - N_z) M_z - \frac{6K_1}{M_z} \sin^2\theta \cos^2\theta \right) \right]$$

The demagnetizing factors Nx, Ny and Nz for a plane surface are substituted into (48) giving

$$(49) \quad \omega^2 = \gamma^2 \left[\left(H_z + 4\pi M_z + \frac{2K_1 \sin^2\theta}{M_z} \right) \left(H_z - \frac{6K_1}{M_z} \sin^2\theta \cos^2\theta \right) \right]$$

We may now use (49 to calculate a theoretical curve which we can compare with our experimental curve.

In calculating this theoretical curve, we shall use a value of $K_1 = 2.94 \times 10^5$ ergs / cm.^{3}, which was determined by Kropschot[5].

---

5. R.H.Kropschot, Master's Thesis, Michigan State College, (1950)

III. Arrangement of Apparatus and Calibration Procedures

Before we discuss the apparatus of this experiment in detail we shall consider an overall description, accompanied by a block diagram which is shown on the next page.

The system consists of a Shepherd-Pierce 723A/B Klystron oscillator, wave guide sections, a cavity wavemeter, a squeeze section, directional couplers, crystal rectifiers, an audio amplifier, an oscilloscope, and power supplies for the microwave oscillator.

The r.f. power source was the Shepherd-Pierce Klystron at a frequency of about 9375 mc./sec. The voltage to the resonant cavity is supplied by a 300 volt regulated power supply. The repelling electrode of the Klystron is modulated by an audio frequency square wave which is superposed upon a variable negative D.C. voltage which attains a negative maximum of about -200 volts. The Klystron filament voltage is supplied by a 6.3 v. secondary from a 60 cycle, 110 volt transformer.

The power generated in the oscillator is coupled, by means of a coaxial probe, into a 3 cm. rectangular waveguide. The power then flows through a cavity wavemeter which is in turn coupled through the waveguide to a variable "flap" attenuator, whose function is to decouple the load from the oscillator and prevent load changes from varying the oscillator frequency.

The next component in the microwave circuit is a squeeze

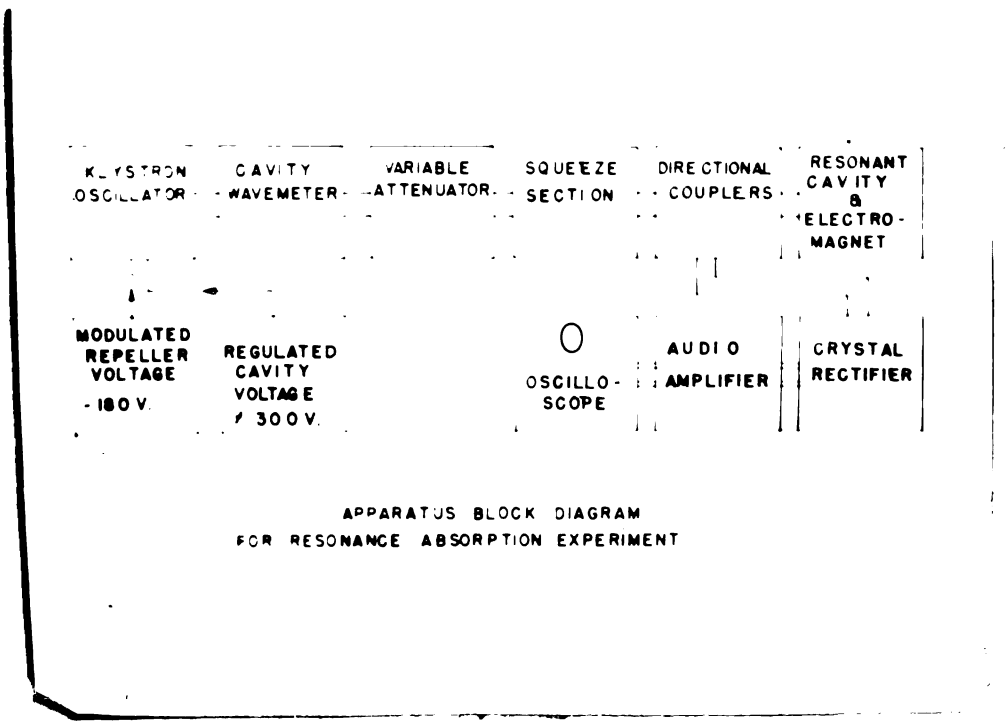

APPARATUS BLOCK DIAGRAM
FOR RESONANCE ABSORPTION EXPERIMENT

Figure 9 Apparatus Block Diagram

section. Its function is to change the electrical length of the waveguide. This process serves to give the load a better impedance match with the oscillator.

Going from the squeeze section, away from the oscillator, we have two directional couplers, represented by a single block in the diagram. The directional couplers are oriented in such a manner that they provide us with a means of viewing the transmitted and reflected waves. The coupler oriented to couple out the reflected wave is the one used most since we measure power reflected from the waveguide termination.

From the directional couplers, we have two branches. One is the main waveguide which terminates in a resonant cavity. The other branch goes to a crystal rectifier, which sends the detected waves, via coaxial cables, to the audio amplifier.

The audio amplifier receives a rectified square wave minus the r.f. component. From the audio amplifier, the amplified square wave is coupled, again via coaxial cable, to an oscilloscope where the square wave can be viewed visually.

Having discussed the coupling of the transmitted and reflected waves from the directional couplers, let us follow the progress of the power from the couplers down the waveguide to our resonant cavity. The field components travel through the main waveguide to the resonant cavity.

The resonant cavity consists of an iris in the waveguide, plus, of course, the waveguide termination. The iris is mounted perpendicular to the direction of propagation and is about 1/3 of the narrow dimension of the waveguide in diameter.

The length of the resonant cavity is one guide wavelength (or multiples of $\lambda g/2$) and can be varied depending on whether we have a variable or a fixed cavity. A variable cavity would be achieved by means of a movable shorting plunger as the waveguide termination.

The ferromagnetic sample is situated as follows: In the case where we have a variable cavity, the sample forms part of the wall of the guide in the narrow dimension, and when the cavity is fixed, the sample is usually placed as a termination on the waveguide.

The last section of our block diagram is shown as the electromagnet. The polepieces are adjacent to the long dimensions of the guide i.e. they are parallel to the long dimension. The sample is always directly between the polepieces.

The strength of the magnetic field between the polepieces is varied by varying the D.C. current through the coils. This current is measured with a D.C. milliameter in the coil circuit. The field is calibrated as a function of oersteds vs. current through the magnet's coils. This process will be described later.

The cavity wavemeter was calibrated to give a curve of wavemeter setting (C.W.S.) versus wavelength. This process sill also be described later in the report.

Having given a general description of the entire apparatus used in the problem, we will now discuss, in more detail, specific pieces of apparatus.

POWER SUPPLIES AND VOLTAGE REGULATION

Since the stability of a reflex Klystron oscillator is dependent on very well-regulated voltages, it was necessary to devote a considerable amount of time on building a well-regulated power supply for the system.

Before we discuss the power supplies used in this experiment, let us outline briefly the requirements of a Shepherd-Pierce tube:

A positive, well-regulated, D.C. Voltage, which can be varied from two hundred to three hundred and fifty volts, is necessary for the resonant cavity of the tube. Also, a steady, negative D.C. voltage, upon which is superposed a well-regulated square wave form, is required for the repeller electrode of the 723 A/B.

Before we enumerate technical details of the power system, let us give a brief resume of the action taken:

We had at our disposal a square wave generator which gave an unregulated waveform. To eliminate the effects of the non-regulated square wave, the experimenter coupled this waveform into a two stage audio amplifier consisting of a simple resistance, coupled stage and a cathode follower stage. The resistance coupled stage was driven to saturation and cutoff and clipped the top and bottom of the waveform off. Since the two stage amplifier was driven by regulated voltages, the operation of the resistance coupled stage eliminated the effect of the lack of regulation in the original square wave generator. The cathode follower stage was an attempt to affect an

impedance match between the repeller electrode and the square wave generator.

The square wave output from the cathode follower was superposed on a negative battery voltage which went to a potential divider and thence to the repeller electrode of the reflex Klystron. The battery voltage was obtained from a bank of storage batteries.

The power supply and voltage regulator supplying voltage to the two-stage amplifier and to the resonant cavity were of this nature:

The power supply consists of a 5U4-G full-wave rectifier connected to the secondary of a step-up transformer. The filter is a conventional condenser-input pi-type filter.

The output of the power supply goes to an electronic voltage regulator. This regulator consists of a regulator and a control tube, one being in parallel with the D.C. output voltage and the other in series. The effect is that the control tube (the one in parallel) furnishes bias voltage to the grid of the series tube which acts as an automatic variable resistor. If the voltage output increases, current through the series tube increases and causes a more positive voltage to be placed on the control grid of the parallel tube. This tube conducts more and therefore its plate voltage drops which makes the grid of the series tube more negative and tends to decrease the current flow through it, thus lowering the output voltage.

A schematic diagram of the power supply and voltage regulator is shown on page 23. The schematic of the two-stage

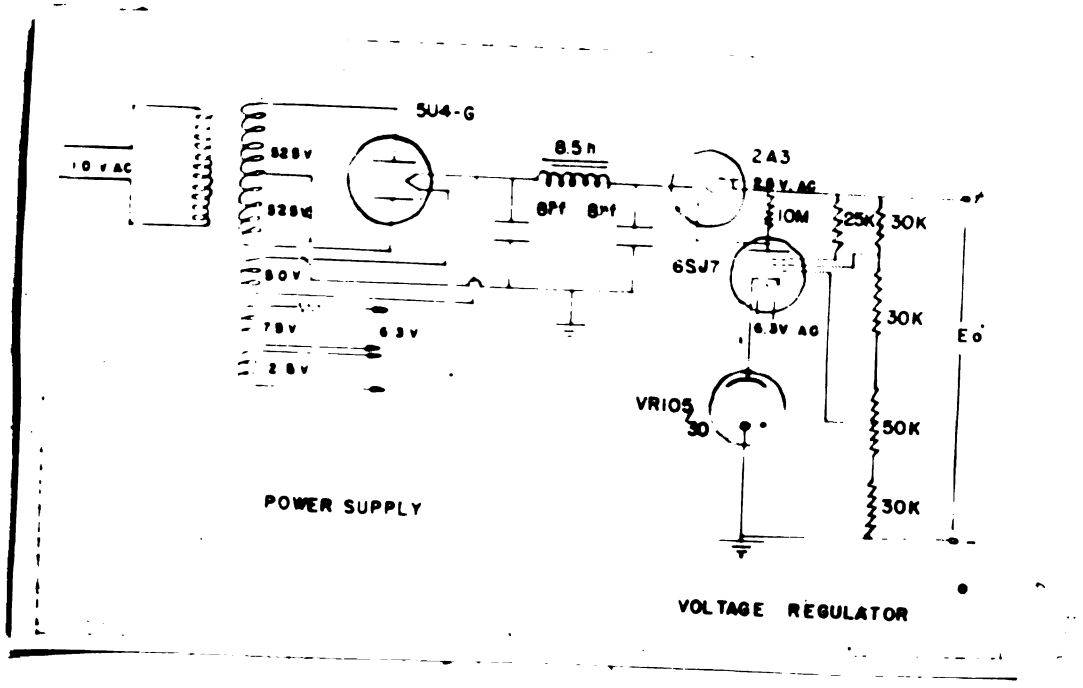

Figure 10 Schematic Diagram of Power Supply and Voltage Regulator

amplifier is omitted because of its simplicity and conventional design. This amplifier is on the same chassis as the power supply.

THE DIRECTIONAL COUPLER

A directional coupler is a device which couples power from a waveguide and is able, at the same time, to differentiate between a transmitted and reflected wave. A description of this function will follow after an analysis of the construction of the instrument.

A single hole ("Bethe-Hole") coupler was used and is constructed as follows: Two sections of waveguide are fastened together with their long dimensions adjacent. There is a single common hole connecting the waveguides as this drawing illustrates:

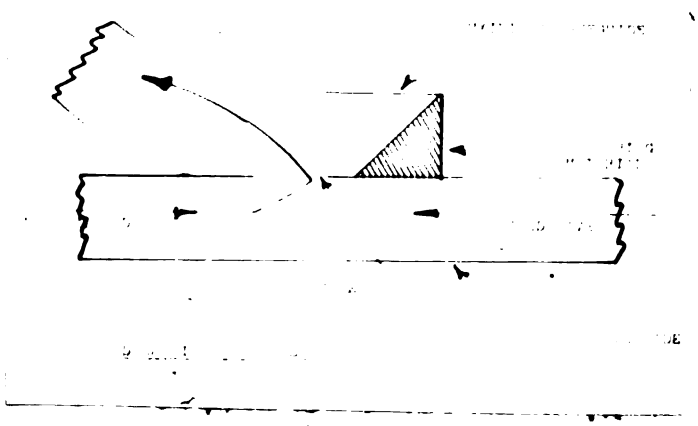

Figure 11

We assume an electromagnetic wave incident from an oscillator on the left side of the diagram. Power will couple into the auxiliary waveguide in a backward direction as shown. Some power will be coupled in the forward direction and will be absorbed by the absorbing material placed there. The

reflected wave, incident from the right, will not couple into the auxiliary waveguide in any appreciable amount.

We shall now define incident power as P_i, power coupled in a useful direction as P_f and power absorbed by the absorbing material as P_b. Using these quantities we will mathematically define some properties of the "Bethe-Hole" coupler.

Directivity is an indication of the quality of a coupler and is given, in decibels, as

$$(50) \quad D = 10 \log_{10} \left(\frac{P_f}{P_b} \right)$$

where P_b approaches zero in the ideal case.

Coupling gives an indication of the ratio of power incident from the oscillator to useful power coupled into the auxiliary guide (P_f). Coupling is given by

$$(51) \quad C = 10 \log_{10} \left(\frac{P_i}{P_f} \right)$$

and is also in decibels.

We now consider how coupling takes place through the hole. The power coupled into our auxiliary waveguide is a superposition of two electric fields outside the hole, one produced by the electric field in the guide and the other produced by the magnetic field in the waveguide. Consider the drawing

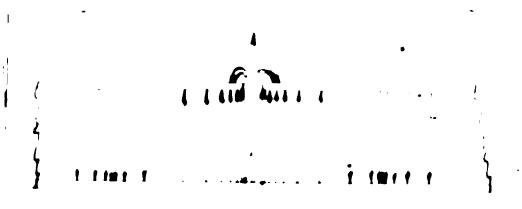

Figure 12

Figure 12 represents electric field coupling through the hole, where the field coupled through the hole is exactly analogous to an oscillating electric dipole.

The magnetic field coupling is illustrated thusly:

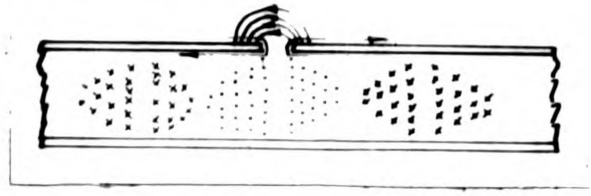

Figure 13

The dots and crosses, of course, mean lines of force going into and coming out of the plane of the paper.

In the magnetic field coupling, the electric lines of force coupled into the auxiliary guide are set up by a flow of current inside and outside the hole. This current flow induces charges on the outside of the hole which set up the electric field lines as shown. We shall now illustrate the superposition of the two fields.

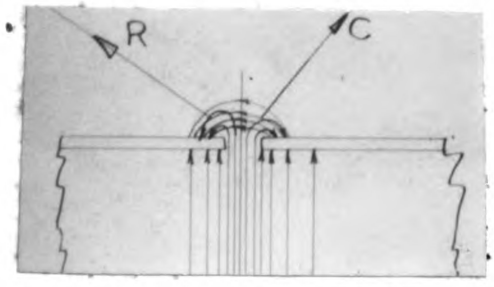

Figure 14

One can easily see that there is partial reinforcement to the left and partial cancellation to the right as shown by the vectors R and C.

This discussion is valid for the TE_{10} mode only, which

is used predominately in microwave work.

It is obvious that one has simply to orient the directional couplers properly to view either transmitted or reflected radiation in a waveguide. Should one be viewing transmitted radiation, he has but to turn the coupler through 180° to view reflected radiation. There are dual purpose couplers which have two auxiliary guide arms and enable one to view reflected and transmitted waves simultaneously.

CAVITY WAVEMETER CALIBRATION

An interesting problem which arose in this experiment was that of calibrating our cavity wavemeter. The cavity wavemeter used has a scale which varies from 0 to 18 arbitrary divisions and it was this scale which had to be calibrated against wavelength in free space. This calibration gave us a means of knowing the frequency passing through the wavemeter by referring to the calibration curve. Before we discuss the apparatus used in this calibration, we must study the waveguide wavemeter and its uses.

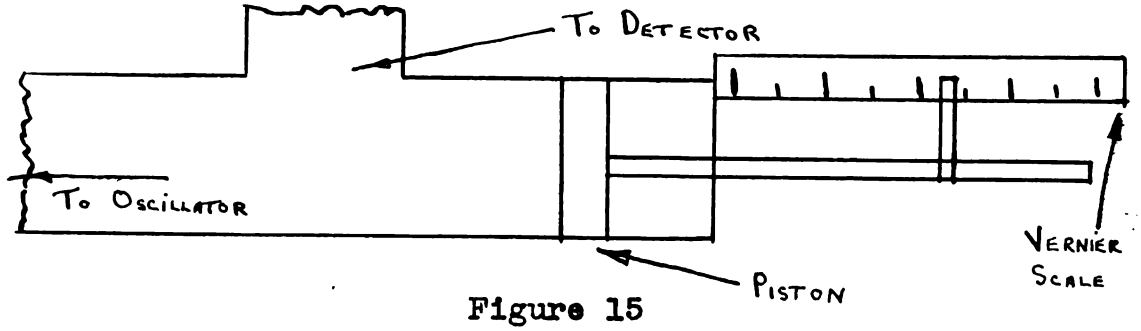

Figure 15

The waveguide wavemeter[6] consists of an H plane "T" junction, a piston to push along the waveguide, and a vernier scale for measuring the distance the piston has moved. A

6. A.B.Pippard, Journal of Scientific Instruments and of Physics in Industry 26 ,296(1949)

microwave oscillator is coupled to the waveguide as shown and the side arm of the guide is coupled to a detector and a standing wave is set up in the waveguide.

The purpose of this apparatus is to measure half-wavelengths in the guide by moving the piston. The section between the detector and the piston end of the waveguide is made long enough so that the piston can be moved through about a half-dozen half-wavelengths and a mean $\lambda_g/2$ can be computed.

From the theory of electromagnetic waves, we learn that two boundary conditions must be met by this moving piston

1) The tangential electric field must be zero at the boundary of the piston.

2) The magnetic field must be a maximum at the boundary of the piston.

These conditions must always be met, so when the piston is moved, the above conditions must hold and the standing wave pattern will be moved down the waveguide. The waveguide arm to which the detector is coupled then receives a varying magnetic field (since only magnetic coupling will take place) and if suitable indicating apparatus is provided, one can tell visually when the minimum position of a standing wave pattern is at the detector. Thus, as we discussed earlier, one can move the piston and get consecutive minimum positions of the standing wave pattern at the detector.

We may now discuss the arrangement of apparatus and the experimental procedures employed in calibrating the cavity

wavemeter. The block diagram of apparatus is shown on page 30.

The microwave power from the Klystron is coupled through a waveguide section to the cavity wavemeter. From the cavity wavemeter the power goes to our waveguide wavemeter. Power is coupled to a crystal detector from the waveguide wavemeter. From the detector the detected power goes to an audio amplifier and thence to an oscilloscope. Since the Klystron is modulated with a 60 c.p.s. square wave we can view the detected pulse on our oscilloscope. When the piston in the waveguide wavemeter is moved, we can observe the pulse on the oscilloscope screen go through successive maxima and minima. By taking the difference between successive readings on the vernier scale when the oscilloscope pulse is at a minimum, we obtain a half-wavelength in the waveguide, given by $\lambda g/2$. We can relate λg to the wavelength in free space by the formula

$$(52)\quad \lambda_a^2 = \frac{\lambda_g^2}{1 + \left(\frac{\lambda_g}{2a}\right)^2}$$

where a is the long dimension of the waveguide.

To calibrate the cavity wavemeter, one must set the cavity wavemeter at a setting and adjust the frequency tuning controls of the Klystron for maximum pulse size on the oscilloscope. After these adjustments have been made, it may be necessary to vary the cavity wavemeter setting somewhat to obtain the best maximum pulse size on the oscilloscope. One then uses the outlined method for finding the λg. It is best to start at one end of the scale and employ this procedure over the entire scale, trying to get at least twenty readings of

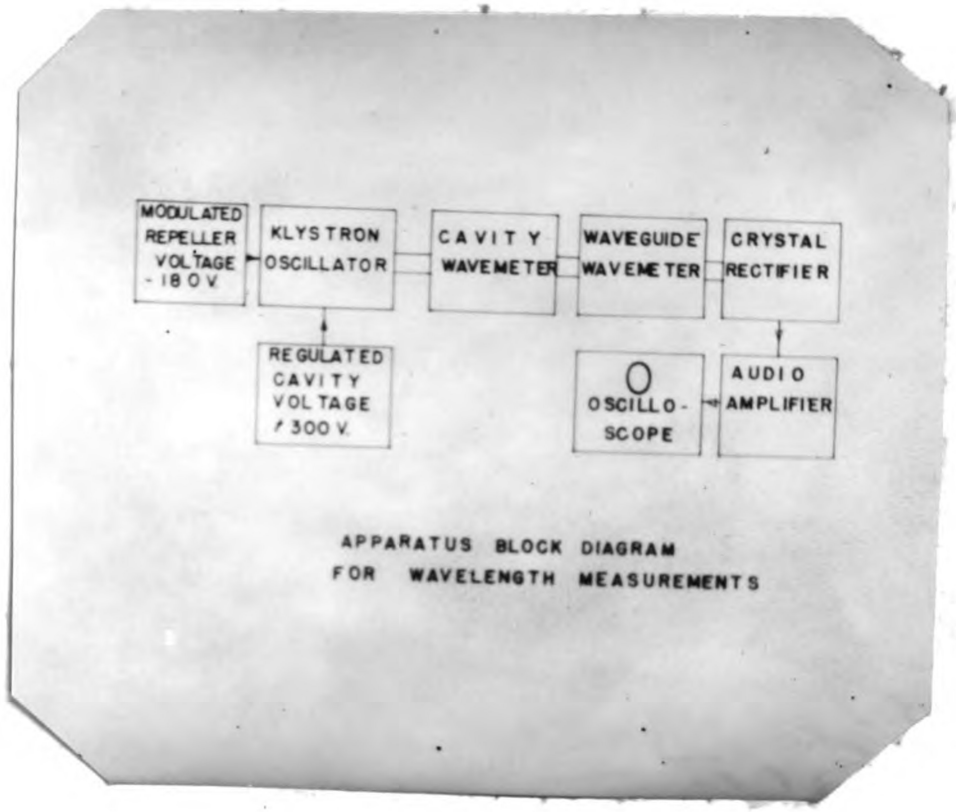

Figure 16 Block Diagram of Wavelength Measurement Apparatus

λg vs. C.W.S. This many readings will give a good curve if carefully taken. The curve obtained for the cavity wavemeter used in this problem is shown on page 32.

A discussion of wavelength measurements using the waveguide wavemeter would be incomplete without a discussion of error involved in the measurements.

From equation (52), one transforms λg to λa, and observes that

$$(53)\quad \frac{1}{\lambda_a^2} = \frac{1}{\lambda_g^2} + \frac{1}{(2a)^2}$$

or

$$(54)\quad (\lambda_a)^{-2} = (\lambda_g)^{-2} + (2a)^{-2}$$

We can differentiate this and obtain

$$(55)\quad \frac{-2\,d\lambda_a}{(\lambda_a)^3} = -\frac{2\,d\lambda_g}{(\lambda_g)^3} + \frac{+4\,da}{(2a)^3}$$

Now if we change the signs of (55) and multiply by λ_a^2, the result is

$$(56)\quad \frac{d\lambda_a}{\lambda_a} = \frac{d\lambda_g}{\lambda_g}\left(\frac{\lambda_a}{\lambda_g}\right)^2 + \frac{da}{a}\left(\frac{\lambda_a}{2a}\right)^2$$

In (56), $\frac{da}{a}$ is proportional to the % error in the measurement a of the waveguide, $\frac{d\lambda_g}{\lambda_g}$ is prop. to the % error in λg, and $\frac{d\lambda_a}{\lambda_a}$ is proportional to the % error in λ_a. The precision of λg can be made very high by taking many measurements. In most cases the dimension a can be known accurately to within .001 or.002 cm. This measurement is the limiting accuracy of the measurement of λ_a since λ_a can be known no more accurately

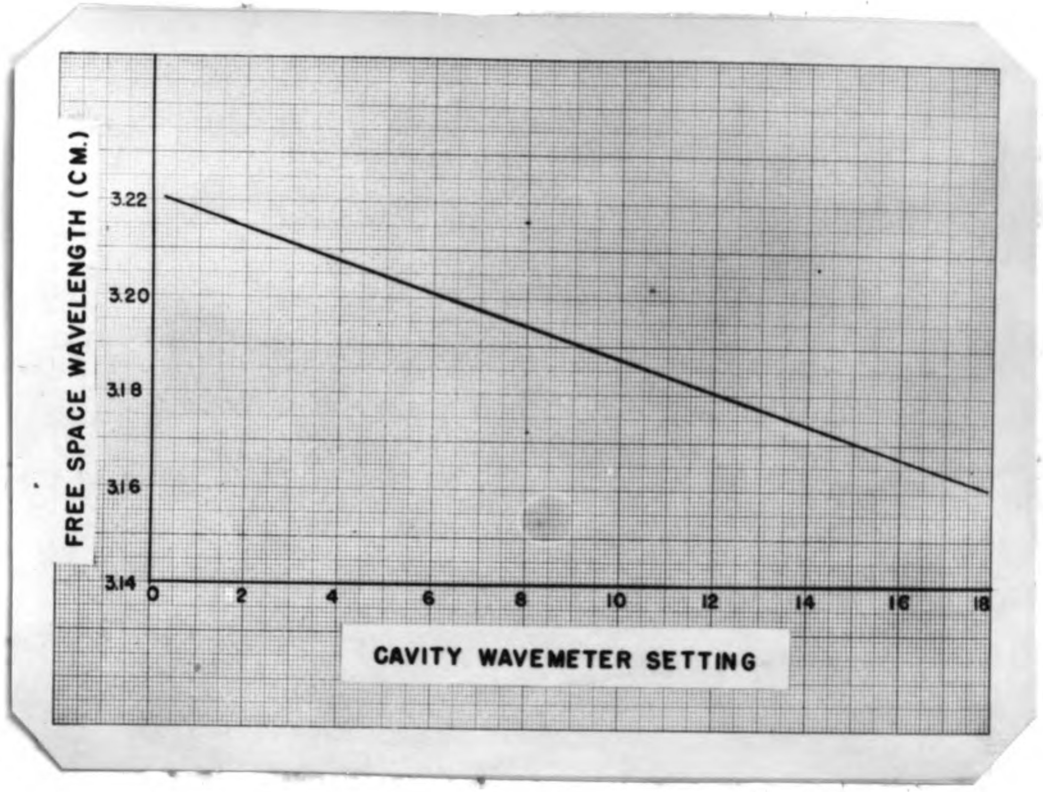

Figure 17 Calibration Curve for Cavity Wavemeter

than the worst factor in the calculation i.e. the measurement of the dimension a. Therefore, this wavelength measurement is limited in accuracy by the dimensions of the waveguide, which are not too accurately known.

MAGNETIC FIELD CALIBRATION

The magnetic field used in this experiment had to be known with a fair degree of accuracy. This was accomplished by placing a milliameter in the coil circuit and making a calibration curve of current through the coils versus magnetic field in gauss. The curve obtained for our particular magnet with the particular polepiece separation used is shown on page 34. The field values were ascertained by measuring the flux with two fluxmeters and, since the meters were in very close agreement, accepting the mean of their readings as a correct field value.

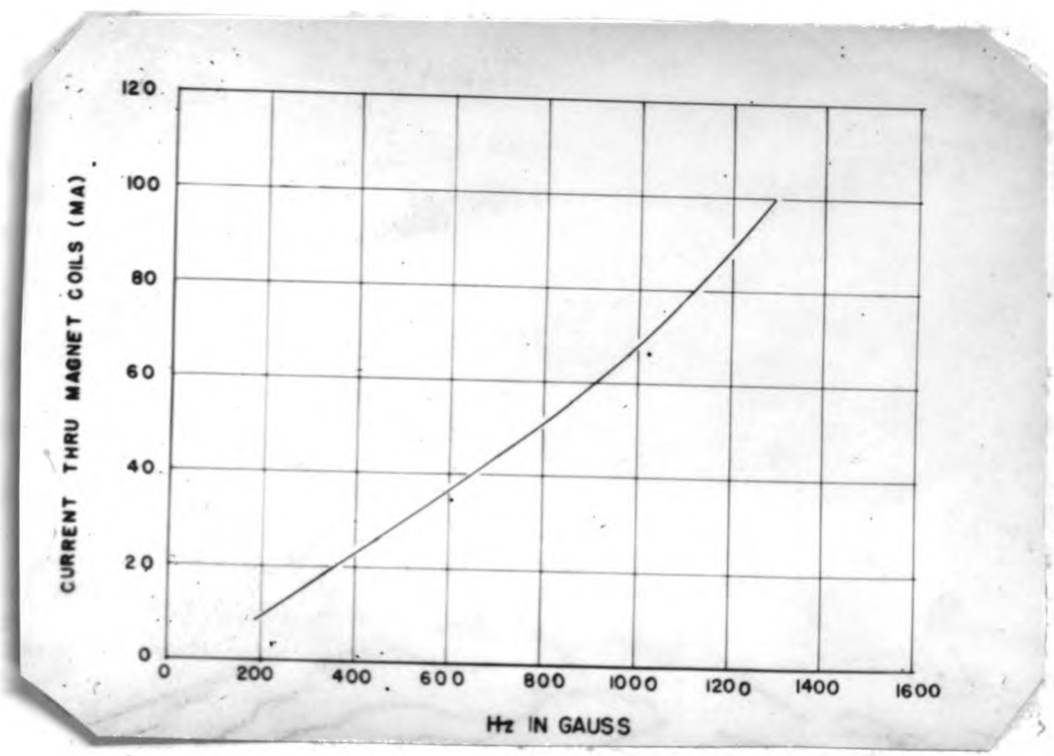

Figure 18 Curve of Magnetic Field of Electromagnet versus Current through the Magnet's Coils

IV. Experimental Procedure

The experimenters used various methods to observe ferromagnetic resonance absorption. The first one we shall describe is one in which a fixed resonant cavity was employed. The length from the iris to the sample was exactly one guide wavelength. The sample was used as a termination for the cavity. We chose a guide wavelength corresponding to a frequency of 9375 mc./sec. The cavity was supposedly accurate to .0005" in length.

This fixed cavity method proved unsatisfactory for reasons which are not apparent. It would seem that when the resonant frequency of the cavity was reached there would be a sharp decrease in reflected power from the cavity. This was not observed. Therefore, the resonance effect was very small and we had to rely on other methods to get a measureable absorption.

The best method was that of using a variable cavity. The iris formed the oscillator end of the cavity and a movable shorting plunger was attached to the end of the waveguide, making up the other end of the cavity. The resonance point could be very easily found by adjusting the shorting plunger. Absorption could be observed only when the cavity was tuned to resonance. It should also be mentioned that this cavity was placed in the microwave circuit as shown in the block diagram on page 18.

One difficulty with this variable resonant cavity was that the machining requirements for the plunger were very exacting

and are usually not met. Therefore, the r.f. losses in the cavity lower the Q considerably and, consequently, the resonance absorption is reduced.

Having discovered the best method for measuring the effect, we now sought a satisfactory way of mounting the ferromagnetic samples in the waveguide. A circular hole was drilled in the narrow dimension of the waveguide, between the iris and the shorting plunger. A rectangular piece of the sample was then cut so that its narrow dimension was just a little less than the narrow side of the waveguide. The sample was then etched in a solution of 1 part H_2O to a part HNO_3(conc), for 15 seconds at 20° C. A brass screw was then soldered to the sample and the sample was inserted into the guide. The screw was inserted through the hole and, by means of brass washers and a brass nut, the sample was firmly screwed into position. A very tight connection between the sample and the guide wall was found to be an absolute necessity if reliable results are to be expected. The drawing below illustrates the arrangement of the sample in the cavity:

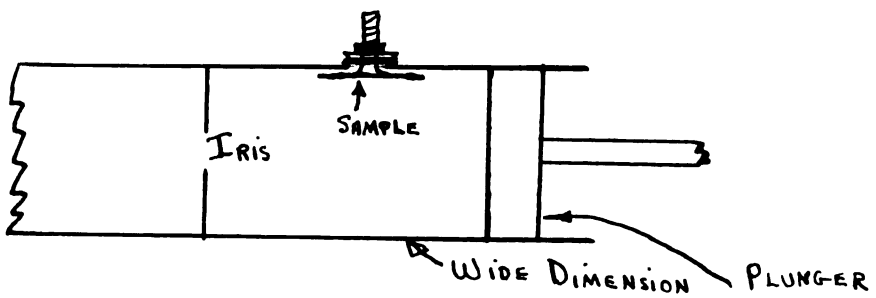

Figure 19

A discussion of the experimental procedure involved would be incomplete without a mention of the type of metal

used, and the method of cutting the samples.

The metal used was furnished by the Allegheny-Ludlum Steel Corporation. The metal is SILECTRON and is a highly anisotropic, polycrystalline iron. The directions of the crystal axes were furnished by the company.

Samples of this metal were cut at specific angles of the 100 direction to the direction of the applied static magnetic field H_z. The angles were 0, 15, 30, 45, 54, 60, 75, and 90 degrees. The field strength of the magnet was varied by changing the current through the coils as we described previously. The resonance was observed by watching the power reflected from the cavity rise and fall as the absorption goes through a maximum. This power change was observed in the change in size of the pulse on the oscilloscope. The easiest way of getting points on the resonance curve is to take readings of magnetic field strength for integral or half-integral changes in pulse height on the 'scope. This is possible since the oscilloscope screen is ruled into squares. Of course, it is necessary to record field strengths on both sides of the absorption maximum.

From theory one learns that each sample of Silectron, oriented in a particular direction, will have a particular resonance field which should be quite different from other angles of orientation. It is this theoretical fact that we have endeavored to check in this problem.

We took about twenty readings of H_{res} for each sample and recorded the mean resonance field for each orientation.

We observed resonance in five or more different samples for each of the eight angles we selected. We found resonance fields for approximately 50 samples.

We then plotted a curve of Resonance Field vs. Angle of Orientation to demonstrate the anisotropy of iron.

An individual curve of Power Absorbed vs. H_z has also been included in this thesis.

V. Data and Interpretation

The data we have obtained is embodied in the one graph of H_{res} vs. Angle of 100 direction to H_z found on page 40. We are also including a graph of H_z vs. Power Absorbed for a single sample of Silectron. This curve illustrates beautifully the resonance peak of power absorption as the static magnetic field is increased. This curve will be found on page 41.

The theoretical curve, calculated from equation (49), agrees quite closely with the experimental curve. The curves are of the same general shape. Their field values differ somewhat, but this may be due to inaccurately calibrated field values.

The anisotropy of polycrystalline iron has been demonstrated by this experiment and the results do not differ greatly from those for a single crystal of Fe as obtained by Kip and Arnold.

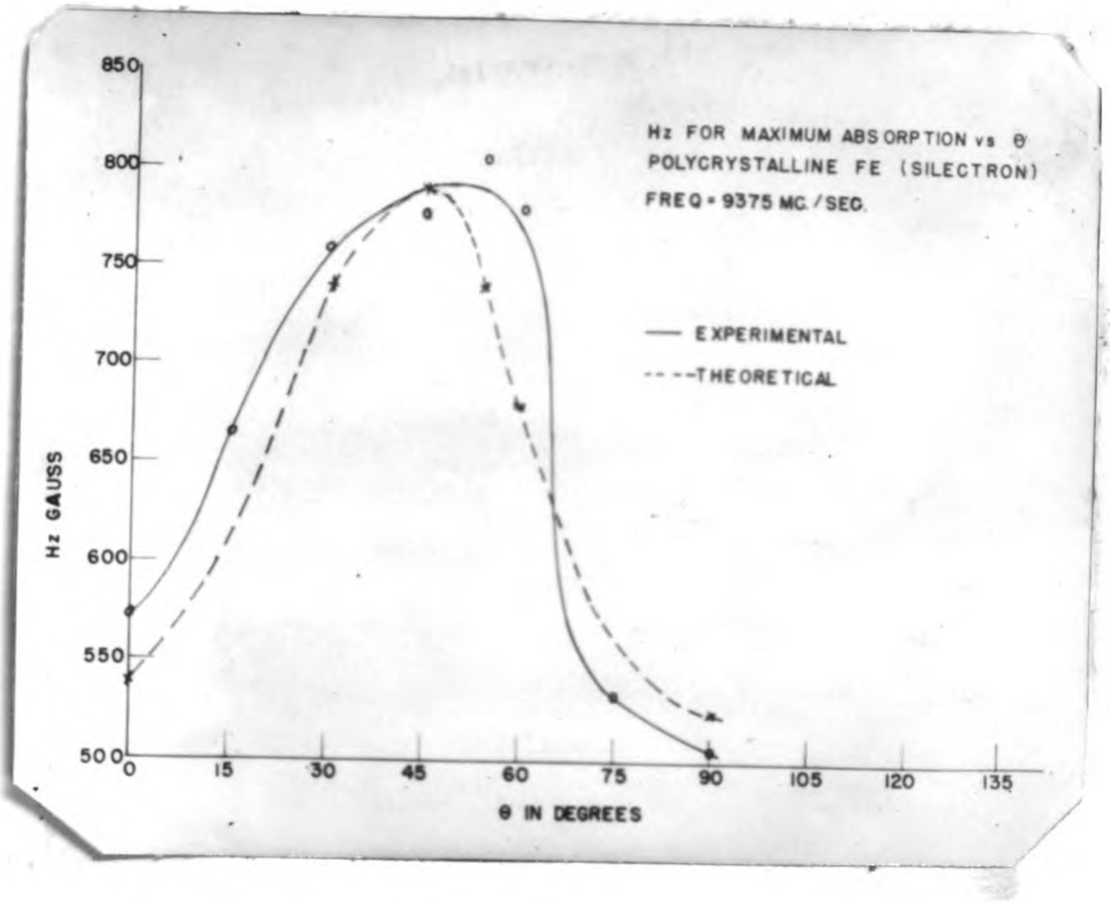

Figure 20 Curve of H_{res} vs. Angle of 100 Direction to H_z for SILECTRON

Figure 21 Curve of Power Absorbed vs. H_z for a sample of SILECTRON